PNAS RESEARCH ARTICLE | EARTH, ATMOSPHERIC, AND PLANETARY SCIENCES OPEN ACCESS

Anthropogenic climate change impacts exacerbate summer forest fires in California

Marco Turco[a,1], John T. Abatzoglou[b], Sixto Herrera[c], Yizhou Zhuang[d], Sonia Jerez[a], Donald D. Lucas[e], Amir AghaKouchak[f,g], and Ivana Cvijanovic[h]

Edited by James Randerson, University of California, Irvine, CA; received September 2, 2022; accepted May 9, 2023

Record-breaking summer forest fires have become a regular occurrence in California. Observations indicate a fivefold increase in summer burned area (BA) in forests in northern and central California during 1996 to 2021 relative to 1971 to 1995. While the higher temperature and increased dryness have been suggested to be the leading causes of increased BA, the extent to which BA changes are due to natural variability or anthropogenic climate change remains unresolved. Here, we develop a climate-driven model of summer BA evolution in California and combine it with natural-only and historical climate simulations to assess the importance of anthropogenic climate change on increased BA. Our results indicate that nearly all the observed increase in BA is due to anthropogenic climate change as historical model simulations accounting for anthropogenic forcing yield 172% (range 84 to 310%) more area burned than simulations with natural forcing only. We detect the signal of combined historical forcing on the observed BA emerging in 2001 with no detectable influence of the natural forcing alone. In addition, even when considering fuel limitations from fire-fuel feedbacks, a 3 to 52% increase in BA relative to the last decades is expected in the next decades (2031 to 2050), highlighting the need for proactive adaptations.

anthropogenic climate change | forest fires | California

Significance

The ongoing intensification in forest fire activity in California has had a dramatic impact on human activities and ecosystems alike. While an increase in temperatures and dryness has been identified to be one of the major drivers of increased summer forest burned area (BA), the extent to which such changes are due to natural variability or anthropogenic climate change remains unresolved. Using the latest simulations for climate change attribution and detection studies and accounting for the uncertainties arising from the data-driven climate-fire model and climate models, we quantify the influence of anthropogenic climate change on recent changes in BA. We show that nearly all of the observed increase in BA over the past half-century is attributable to anthropogenic climate change.

Over the past 50 y, the area burned by summer wildfires in California has been increasing (1). The 10 largest California wildfires all happened in the last 20 y, five of which occurred in 2020 and eight after 2017 (2). Besides their immense environmental impacts, these fires have also had widespread negative impacts on human health and mortality and numerous socioeconomic consequences (3–5).

Recent changes in forest wildfire regimes across the western United States (1, 6–11) are a consequence of complex interactions among climatic and nonclimatic drivers. A number of mechanisms linking climate change to wildfires have been suggested, including below-average precipitation (12–14), higher spring temperatures and low spring snowpack (8, 12), hotter summer temperatures and larger vapor pressure deficit (VPD; 12, 15–17), more frequent hot temperature extremes (18), and a decrease in the number of rainy days during the fire season (19). Nonclimatic factors that have been implicated in changing wildfire characteristics include land management that has facilitated fuel buildup which favors increased burn severity as well as both increased susceptibility of California's aging power grid to extreme weather and increased development in fire-prone areas that changes ignition patterns and fire management (3, 20–29). However, beneath these "external" factors, natural climate variability also influences the occurrence and severity of forest wildfires, creating a noise that can mask the signal of anthropogenic impacts on wildfire changes (30–32).

While understanding and quantifying the relative roles of these individual drivers is of societal importance, rigorous quantification of California's wildfire increases attributable to anthropogenic climate change has been challenging. Important steps in this direction have been made by attributing the anthropogenic impacts on meteorological variables known to be of importance for wildfires or fire risk indices (for example, VPD; 1, 6, 31). Abatzoglou and Williams (6) and Williams et al. (1) used climate model simulations from the fifth phase of the Coupled Model Intercomparison Project (CMIP5; 33) to assess the impact of anthropogenic forcing on increased forest fire activity in the western United States and California, respectively. These studies estimate the role of anthropogenic climate change on observed fire record by removing a long-term low-pass filtered time series from climate models from observed climate data to approximate a counterfactual observational record that does not include the influence of anthropogenic forcing. However, in doing so, these approaches do not faithfully account for the natural climate variability as in standard attribution studies (see e.g., refs. 31 and 34–37). Instead, using historical

Author contributions: M.T., S.H., S.J., A.A., and I.C. designed research; M.T., J.T.A., S.H., Y.Z., and D.D.L. performed research; M.T., J.T.A., S.H., Y.Z., S.J., D.D.L., A.A., and I.C. analyzed data; and M.T., J.T.A., S.H., Y.Z., S.J., D.D.L., A.A., and I.C. wrote the paper.

The authors declare no competing interest.

This article is a PNAS Direct Submission.

[1]To whom correspondence may be addressed. Email: marco.turco@um.es.

This article contains supporting information online at https://www.pnas.org/lookup/suppl/doi:10.1073/pnas.2213815120/-/DCSupplemental.

Published June 12, 2023.

simulations with realistic anthropogenic forcings and simulations with natural climate forcings only can help to better partition temporal variations into internally generated and externally forced components. Such a formal attribution effort is needed to establish the degree to which anthropogenic climate change and natural climate variability have contributed to the increases in burned area (BA) in Californian forests.

Increased temporal coverage of fire datasets by the California Department of Forestry and Fire Protection's Fire and Resource Assessment Program (FRAP) (https://www.fire.ca.gov/what-we-do/fire-resource- assessment-program), covering the period 1971 to 2021 (*SI Appendix*, Table S1), comprehensive long-term meteorological observations, and a large number of state-of-the-art climate simulations developed for climate change attribution and detection studies provide an invaluable resource for investigating the impacts of anthropogenic climate change on wildfire. In this study, we seek to formally attribute the role of anthropogenic climate change on forest fire BA in California and estimate the time when the statistically significant signal of climate influence emerges. We first derive a climate-fire model and run it with the climate data from the Detection and Attribution Model Intercomparison Project (DAMIP; 36), an initiative within the Coupled Model Intercomparison Project Phase 6 (CMIP6; 38). We utilize two sets of simulations: CMIP6-ALL (consisting of spliced historical and SSP2-4.5 scenario runs, that contain all-forcings of the recent past) and CMIP6-NAT (consisting of hist-nat experiments containing natural-only forcing). Our climate-fire model is derived using summer forest BA data for the period 1971 to 2021 and the corresponding climate data. In addition to quantifying the impacts of anthropogenic climate change on forest fires in California since 1971, we complete our analysis by exploring possible future evolutions of California's forest BA during 2031 to 2050 considering a large suite of global climate models and several different versions of climate-fire models under different climate change scenarios (*Materials and Methods*).

Results

Climate-Fire Model. To evaluate the impacts of past climate trends, we first build a model describing the climate-fire interactions over the period 1971 to 2021. We fit all possible regression models considering the logarithm of summer (May to September) forest fire BA and all the potential predictors (maximum temperature, precipitation, and VPD, aggregated over different time windows) together or individually through a leave-one-year-out cross-calibration. The best model, among the different combinations and temporal aggregation of the predictors considered, is the one that considers only the monthly mean of daily maximum near-surface air temperature (TS_{MAX}) averaged over the period from spring to summer (April to October; see *Materials and Methods*).

This is also reflected by the correlations between log(BA) and the different climate variables (*SI Appendix*, Table S2). Specifically, climatic drivers of fuel aridity (high TS_{MAX}, high VPD, and precipitation deficit) are positively related to BA, consistent with interannual climate-BA relationships in biomass-rich regions where fuel abundance is less limiting (38, 39). *SI Appendix*, Table S2 also shows that BA exhibits a stronger correlation with TS_{MAX} or VPD (between 0.71 and 0.84 depending on the variables/aggregation windows) than with precipitation (–0.49 to –0.36), confirming previous studies in primarily flammability-limited regions (see e.g., refs. 1 and 6). This may be explained since little precipitation falls in this region in the spring to summer months (around 22% of the total annual precipitation amount) and also since TS_{MAX} and VPD are better proxies for aridity than precipitation as drier atmospheric conditions affect the fuel moisture content of live and dead trees, affecting fuel availability (40).

Importantly, correlations between climate variables can hamper model development. Including dependent predictors can lead to model overfitting; conversely, excluding some determinants can omit important effects of climate on fires. *SI Appendix*, Table S3 reports the correlations among TS_{MAX}, VPD, and precipitation. There is a high correlation (between 0.90 and 0.95 depending on the aggregation windows) between TS_{MAX} and VPD due to the exponential Clausius–Clapeyron effect of temperature on saturation vapor pressure. In addition, TS_{MAX} and VPD are negatively related to precipitation (correlation coefficients ranging between –0.67 and –0.50) as dry conditions induce near-surface moisture deficits, amplifying sensible heating, and consequently elevating surface air temperatures and evaporative demand (41). Thus, one variable effect on fires may be entrained in the correlation between BA and the other variable. For this reason, we present the outcomes obtained both using the TS_{MAX}-BA model and the model that takes into account the effects of precipitation.

Fig. 1*A* shows the strong relationship between log(BA) and TS_{MAX}. Indeed, the correlation between these two variables is 0.84 (P-value < 0.01). Importantly, the partial correlation between log(BA) and TS_{MAX}, controlling for the co-occurring effects of precipitation, remains strong and significant (0.81, $P < 0.01$). Fig. 1*A* also indicates that the observed BA displayed a striking increase: in the second half of the study period, i.e., over the years 1996 to 2021, the BA shows a fivefold increase compared to the period 1971 to 1995 (1,710 km^2 versus 361 km^2 annual averages). At the same time, TS_{MAX} increased by around 0.8 °C (23.3 °C versus 22.5 °C). It is worth noting that the two seasons with the greatest BA values, i.e., in 2020 and 2021, coincide with the two highest temperature values. Fig. 1*B*, comparing observed and predicted BA, confirms that our simple regression model provides skillful out-of-sample 10-fold predictions of the influence of climate variability on BA. An ensemble of the 10,000 out-of-sample predictions has been used to demarcate the uncertainty bands, defined by the 2.5th and the 97.5th percentiles. The correlation of the data with the out-of-sample 10-fold predictions (r = 0.82, P-value < 0.01) indicates an accurate model performance, while the variance explained by the in-sample model amounts to about 71%. The exponential relationship between BA and TS_{MAX} means that a one-degree increase in TS_{MAX} is associated with a 222% (160 to 294%) increase in BA.

Precipitation should have played some role in regulating recent fire activity and is also projected to change in the future. However, in the case of our TS_{MAX}-BA model, the impact of precipitation is not obvious since it is implied indirectly, through its impact on temperature. For this reason, we also consider a second model that includes the direct effect of precipitation. First, we minimize the impact of precipitation on TS_{MAX} by creating a regression model that links precipitation to temperature and use this model to adjust the observed TS_{MAX} values. Subsequently, we formulate a BA model using precipitation and the adjusted TS_{MAX} values as predictors. In this case, both variables are statistically significant in explaining the variability of fires, and the importance of adjusted TS_{MAX} is larger than the precipitation one (*SI Appendix*, Fig. S2).

To further evaluate potential nonstationarity in the climate-fire relationship that can occur due to exogenous determinants, we demonstrated that models built using various subsets of the data, or considering detrended fire and climate data, return statistically indistinguishable regression parameters suggesting a limited influence of nonclimatic factors in modulating climate-fire relationships during the study period (*SI Appendix*, Fig. S2). We train a model based on the first (1971 to 1995) and second (1996 to

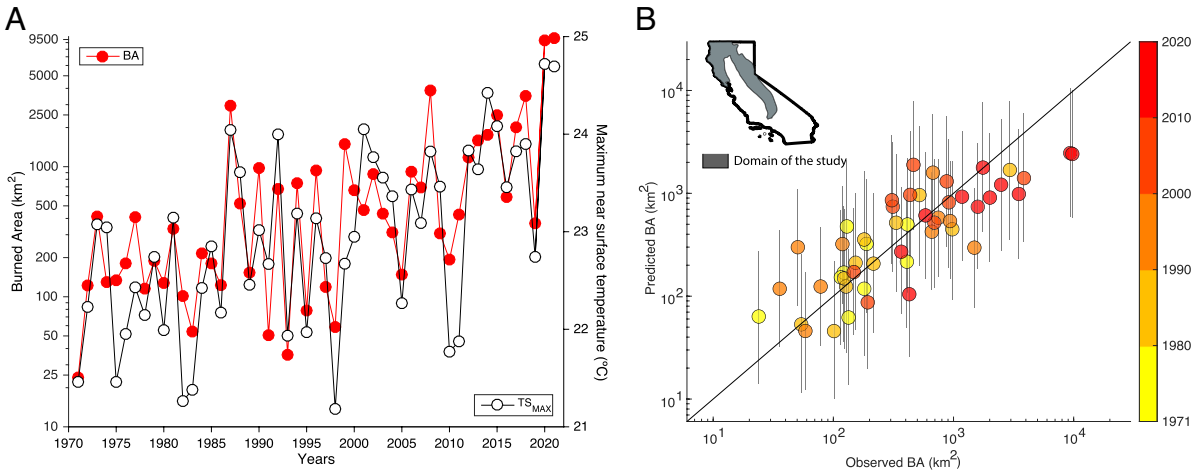

Fig. 1. (*A*) Time series of summer (May to September) forest fire burned area (BA, in red) and spring to summer (April to October) maximum near surface temperature (TS_{MAX}; in black) from 1971 to 2021; (*B*) observed versus out-of-sample 10-fold predicted changes in BA. Vertical gray lines indicate 2.5th and 97.5th percentiles of 10,000 different predictions. Colors indicate the decade of each sample. The *Inset* shows a map of California with the domain of interest shaded in gray.

2021) halves of the studied period and find that the regression coefficient did not change significantly. Similar results were obtained by training the model with the 25 coldest or hottest years (*SI Appendix*, Fig. S2). These tests support fuel aridity (using TS_{MAX} or precipitation and adjusted TS_{MAX} as a proxy) as the leading driver of the interannual variability and trends in forest fire BA in California during 1971 to 2021 and suggest that this model can be used for attribution assessments and offer predictive utility. Forest fires are affected by many interrelated aridity variables besides TS_{MAX} or precipitation and adjusted TS_{MAX}. In this study, these variables are not assumed to be the only factor that affects fire activity but are instead simply treated as a proxy of fuel aridity. In particular, warming is a key driver of the speed at which both live and dead fuels dry out, and thus of fuel aridity and flammability. These findings build upon the previous studies that found a strong relationship between BA and aridity metrics in forested regions in the western United States (see e.g., refs. 1, 14, 39, and 42).

These findings strongly indicate that the observed increase in BA was primarily due to increased fuel aridity and not due to simultaneous variations in nonclimate factors such as human effects on ignitions, fire suppression, or by altering land cover (similarly to the conclusions by refs. 1 and 42). Our results suggest that changes in human environmental factors, including changes in biomass and fire management practices during the period of record, did not significantly affect the stability of the climate-fire relationship at the scales analyzed here. For instance, we assess the solidity of fire-climate relationships during 1971 to 2021 by comparing regression statistics based on only data from 1971 to 1995 versus 1996 to 2021 (*SI Appendix*, Fig. S2). Similar statistical relationships for both periods strongly suggest that nonclimate factors did not cause a change in the fire–climate relationship during the study period. This does not mean that nonclimate drivers had no influence on the contemporary BAs. Contrarily, the twentieth-century buildup of fuels due to fire suppression over the past century (see e.g., refs. 20, 22, 24, and 25) may have influenced the fire–climate relationship in general, heightening the mean state of modern-day forest-fire extent and sensitivity to aridity (20, 21, 23, 24). Thus, although consequences of human activities are apparent in multicentury assessments of fire activity (22, 26, 27), anthropogenic modification in background conditions such as fuel availability throughout our relatively short study period does not emerge as the main driver for the increased in BA during 1971 to 2021.

Attribution of Wildfire BA Changes. To quantify the impacts of anthropogenic climate change on California's forest fire area, we employ the simulations from the DAMIP initiative (36), specifically designed for detection and attribution studies. We run the climate-fire model with the output from climate model simulations using historical forcing that includes both anthropogenic and natural forcing (consisting of spliced simulations of historical "hist" and future "SSP2-4.5" climate experiments, covering the period 1971 to 2021, hereafter referred to as CMIP6-ALL) and using a counterfactual scenario driven by natural forcing alone ("hist-nat"; CMIP6-NAT hereafter). This counterfactual scenario simulates the climate in a world without anthropogenic climate change. A detailed description of the models used is given in the *Materials and Methods* section. Our assessment combines both the statistical uncertainty associated with the climate-fire models, by using 10,000 bootstrap replications, and the climate model uncertainty, by using simulations from different models DAMIP, and internal variability uncertainty, by using different realizations of the same model (*Materials and Methods*).

We found that observed changes in TS_{MAX} and VPD fall within the range of CMIP6-ALL trajectories and not CMIP6-NAT (*SI Appendix*, Fig. S3). The observed TS_{MAX} increase of 0.82 °C between the first (1971 to 1995) and second (1996 to 2021) halves of the studied period is consistent with the change for the CMIP6-ALL experiments (+0.96 °C, 95% CI: 0.73/1.26 °C), while CMIP6-NAT experiments did not show any warming (0.04 °C, CI: −0.64/0.25 °C). Analogously, observed VPD increased by 0.95 hPa, comparable to that of CMIP6-ALL simulations (0.81 hPa, CI: 0.55/0.96 hPa) but not CMIP6-NAT simulations (0.17 hPa, CI: −0.12/0.32 hPa). By contrast, no significant changes in precipitation were evident in CMIP6-ALL (−10 mm, CI: −37/12 mm) and CMIP6-NAT (−0.3 mm, CI: −37/25 mm) experiments or in the observational record (the observed change between the two time periods is −0.2 mm; *SI Appendix*, Fig. S3).

Simulated and observed BA trends over the period 1971 to 2021 are shown in Fig. 2*A*. Models run with combined natural and anthropogenic forcings show a positive trend, similar to the observed one, whereas simulations with natural forcings alone indicate no trend in BA. We estimate the impact of

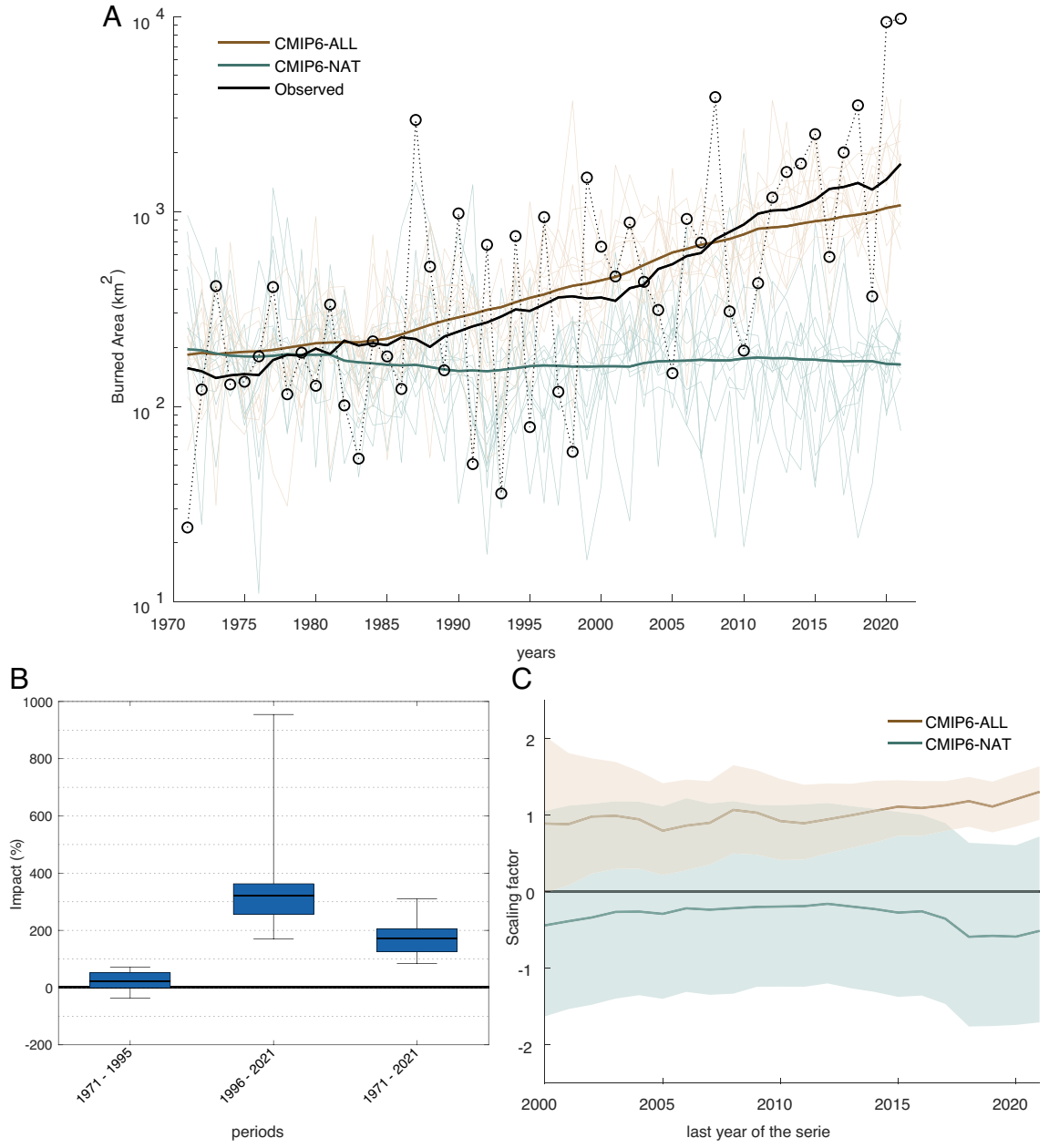

Fig. 2. Attribution of recent climate change considering (*A*) annual BA; (*B*) the impact of anthropogenic climate change on BA as a relative change in BA in CMIP6-ALL compared to CMIP6-NAT over 1971 to 1995, 1996 to 2021, and 1971 to 2021; and (*C*) the scaling factor from the detection analysis. The climate simulations are consistent with the observation if the lower bound of the shaded band is larger than zero. In panel *A*, the black line represents observed 21-y moving average, while dashed lines with open circles show the observed annual values; the brown and green solid lines represent the 21-y moving averages of the ensemble means of CMIP6-ALL and CMIP6-NAT historical experiments, and the thin brown and green lines are for 12 model ensemble means from CMIP6-ALL and CMIP6-NAT, respectively. In *B*, the median is shown as a solid line; the box indicates the 25 to 75 percentile range, while the whiskers show the 2.5 to 97.5 percentile range. In *C*, the brown (green) shaded band shows the 2.5 to 97.5 percentile range of the CMIP6-NAT (CMIP6-ALL) scaling factors. The impact simulations span 10,000 different predictions × 12 GCMs.

anthropogenic climate change on BA as a relative change in BA in CMIP6-ALL compared to CMIP6-NAT over a given period (CMIP6-ALL–CMIP6-NAT)/CMIP6-NAT (Fig. 2*B*). We find that climate simulations that included both human and natural forcings yield 172% more BA (84/310%) during 1971 to 2021 than models without anthropogenic forcing. Interestingly, in the first half of the period studied (i.e., 1971 to 1995), the impact of climate change is relatively small and not significant (+23%, CI: −36% to +71%). However, in the second half of the period (1996 to 2021), the impact is 320% (170/955%).

To quantify when and how much of the observed increase in BA is attributable to climate change, we next regress the multimodel mean BA series from CMIP6-ALL and CMIP6-NAT against the observed BA values, starting with the time period 1971 to 2000 and extending it by one year through 2021 (Fig. 2*C*). The resulting regression coefficients represent the scaling factors that are needed to reproduce the observed trends and quantify the level of consistency between the models and the observations. Values consistent with 1 and with a small uncertainty range indicate good agreement between the models and the observations. The scaling factor for CMIP6-ALL ensemble mean is close to 1 over almost

the entire period, suggesting that the model-based estimate of BA changes is consistent with observations. In addition, the scaling factors for CMIP6-ALL are statistically different from zero since 2001, reflecting that we have "detected" the signal of climate change in the observed BA values after this year. In contrast, for CMIP6-NAT, the scaling factor values are not statistically different from zero, indicating no detectable influence of the natural forcing (when including more years from the last decade, the scaling factor values for CMIP6-NAT become more negative but still not significant at the 95% confidence level). CMIP6-ALL and CMIP6-NAT simulations both feature relatively large uncertainty bands that, as expected, decrease as more years are taken into account. Their respective uncertainty bands overlap for most of the time periods considered; however, starting in 2018, there is a complete separation between CMIP6-ALL and CMIP6-NAT scaling factor distributions suggesting a complete dominance of anthropogenic over natural forcing. We conclude that the observed BA changes are inconsistent with internal variability or natural forcing alone and since 2001 can be attributed to the combination of anthropogenic and natural forcing from CMIP6-ALL simulations. These conclusions are supported when constraining the analysis to the first ensemble member of each climate model (*SI Appendix*, Fig. S4) and also when considering the second climate-fire model that includes the precipitation effect (*SI Appendix*, Fig. S5).

Future Evolution of BA. Given the importance of anthropogenic climate change for the increase in forest BA in California between 1971 and 2021, a critical question is what the future evolution of fires will look like with further changes in climate. The projections of future climate show robust temperature increase in the next decades: TS_{MAX} is projected to increase by 1.4 °C (with +0.7 to +2.0 °C 2.5 to 97.5 percentile range) for 2031 to 2050 compared to 1995 to 2014 using the SSP2-4.5 scenario and by 1.6 °C (+0.8 to +2.6 °C) under the SSP5-8.5 scenario. Precipitation is projected to moderately decrease by −2.5 % (−16 to +11 %) using the SSP2-4.5 scenario and by −3.3% (−16 to 10%) under the SSP5-8.5 scenario. This temperature increase is translated by our TS_{MAX}-fire model into an exponential BA increase (Fig. 3*A*), with an average annual BA for the period 2031 to 2050 of ~4,400 km^2 under SSP2-4.5 scenario (~2,100 to ~6,900 km^2) and ~5,100 km^2 under SSP5-8.5 scenario (~2,000 to ~7,500 km^2). Note that, as a reference, observed BA from 2002 to 2021 equals 2,037 km^2. Very similar results have been obtained with the model that includes the precipitation effects (Fig. 3*A*).

Such a simple approximation may however not be sufficient, since fires remove the fuel needed for subsequent fires, leading to near-term fuel limitations for forest BA (42). Indeed, while our results over 1971 to 2021 showed stationary climate-fire relationships at the scale of our analysis, abrupt reduction in forest extent through increased fire activity may alter such relationships. Thus, we further quantify how the fuel limitation resulting from this potential feedback may modify the future trajectory of fires in response to anthropogenic climate change. The dynamic models that include a range of feedback strengths and durations imposed by fire-fuel feedbacks (*Materials and Methods*) reduce the magnitude of the projected increase in forest-fire area from ~4,400 km^2 (under SSP2-4.5 scenario) to a range from ~2,300 km^2 to ~2,800 km^2, depending on the type of feedback-model (Fig. 3), and from ~5,100 km^2 (under SSP5-89.5 scenario) to a range from ~2,500 km^2 to ~3,100 km^2. The model that takes into account the effects of precipitation shows a somewhat smaller increase (Fig. 3). In any cases, even considering the potential reduction due to fuel feedbacks, anthropogenic climate change provides substantial potential for an increase in BA, emphasizing the importance of future fire management strategies.

Discussion and Conclusions

The ongoing increase in forest fire activity in California has had a dramatic impact on human activities and ecosystems alike. Considering the historical impacts of previous wildfires and the bitter taste of the 2020 and 2021 all-time record fire seasons, this is of immense importance. Using the latest simulations developed for climate change attribution and detection studies and accounting for the uncertainties arising from the data-driven climate-fire model, climate models, and internal climate variability, we have investigated the impact of anthropogenic climate change on the observed increase in BA in California's forests. We detect the signal of combined natural and anthropogenic forcing on the observed BA starting in 2001 while finding the observed BA changes to be inconsistent with internal variability or natural forcing alone. We estimate that from 1971 to 2021, anthropogenic climate change contributed to a +172% increase in BA, with a remarkable +320% increase from 1996 to 2021. In the next decades, even when considering fuel limitations from fire-fuel feedbacks, a further increase in average annual forest BA is expected, ranging from 3 to 52% relative to the mean over the past two decades 2001 to 2021, which also corresponds to the highest record since 1971, highlighting the need for proactive adaptations to limit negative impacts of fire to ecosystems and society.

Further work on this topic, should include additional scenarios for future fire management policies, land use, land cover change, and, eventually, future generations of climate models that integrate fire processes under various climate change scenarios. Our results show that the observed increase in BA in California's forests is consistent with the anthropogenic climate change and unlikely to have resulted from natural variability alone. This represents an important step toward overall accountability of the climate change impacts. As the current state of knowledge suggests, and our results strongly support, immediate action toward mitigating the impacts of global warming alongside intentional proactive land management practices that can improve the resilience of forested landscape to fire (43) will all be necessary.

Materials and Methods

Study Region. The study domain consists of largely forested areas in northern and central California (Fig. 1). This domain was defined following ref. 1, by merging the following Bailey ecoregions: "Sierra Nevada", "Sierra Nevada Foothills", "Southern Cascades", "Klamath Mountains", "Northern California Coast Ranges," and "Northern California Coast". The Bailey ecoregions data were obtained from UNEP's World Conservation Monitoring Centre (last access 12/01/2022) at http://datadownload.unep-wcmc.org/?dataset=Baileys_Ecoregions_of_the_World_1989. In this area, around three-quarters of California's forest-fire area occurred during 1972 to 2018 (1).

Fire Data. BA data were obtained from the California Department of Forestry and Fire Protection's FRAP for the period 1971 to 2021. This dataset provides fire perimeters which we clipped at the boundaries of the regions of interest. Then we select the forest fires by lands classified as forest or woodlands (44) and that have started in the 5-mo window from May to September (using FRAP field ALARM DATE) and the burned-area values are aggregated over these months. Note that around 88% of the total BA in the study region occurred in forested lands.

While the FRAP dataset represents the most comprehensive fire inventory for California, it is not free from uncertainties (7, 45). It contains data since 1878, and it is considered a reasonably reliable source of information of past

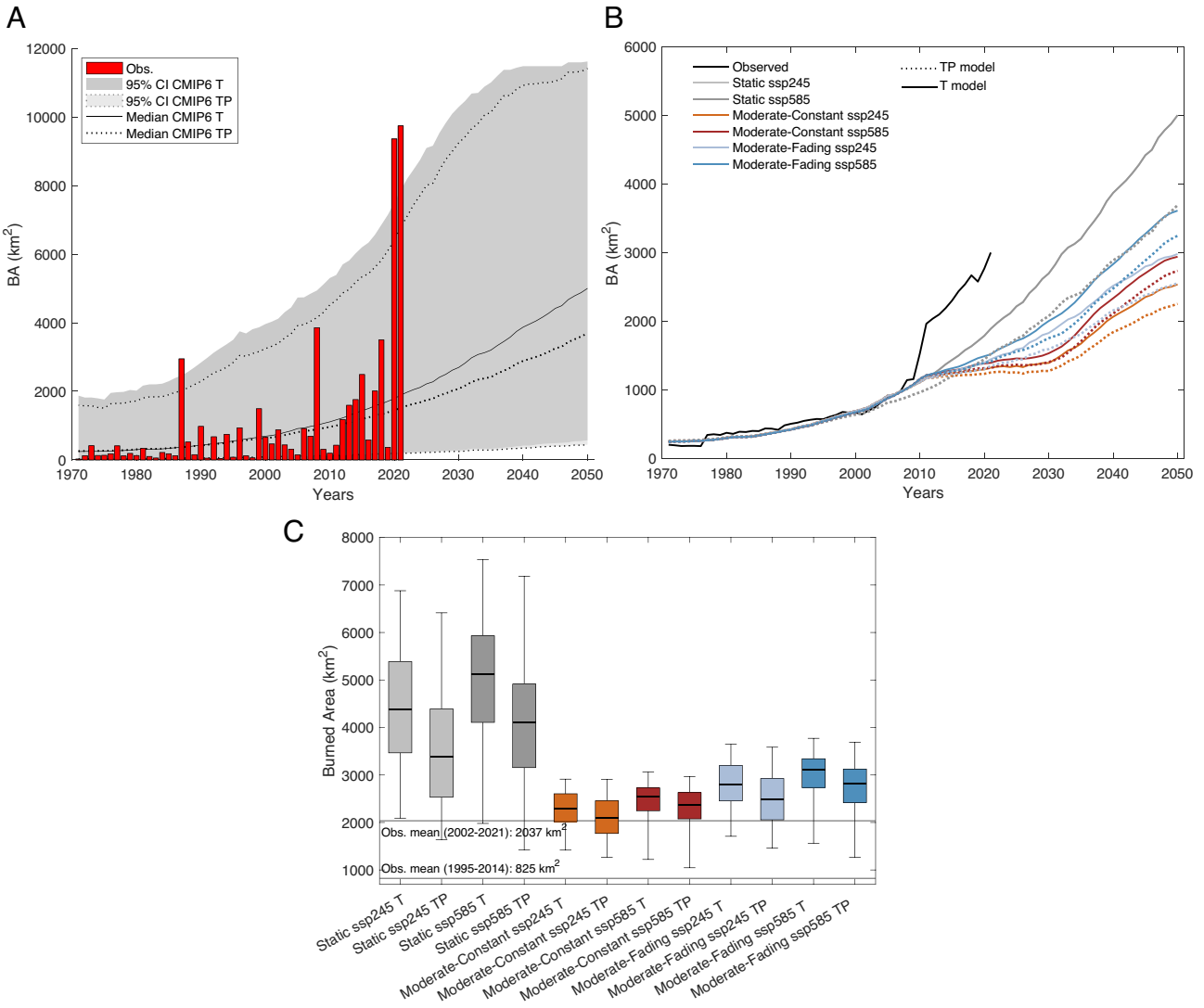

Fig. 3. Forest fire area projections using static and dynamic models. (*A*) Burned areas simulated from CMIP6 climate models and the static climate-fire model (historical forcing until 2014 and SSP2-4.5 forcing 2015 to 2050). Model results are shown as 21-y moving averages to emphasize gradual changes rather than year-to-year fluctuations. Red bars are observations. (*B*) Time series of trailing 21-y moving average considering both static and dynamic models and (*C*) mean burned area in the period 2031 to 2050. The median is shown as a solid line; the box indicates the 25 to 75 percentile range, while the whiskers show the 2.5 to 97.5 percentile range. The BA simulations span 10,000 different predictions × 24 GCMs.

large fires, but it is incomplete prior to 1950 and small fires are frequently missed (45, 46). We constrain our analyses to 1971–201 due to the uncertainty in some of the earlier records and for comparisons with more modern BA data sources. Indeed, we also consult the Monitoring Trends in Burn Severity (MTBS; 47) database and the data used by refs. 1 and 48. Specifically, we consider the BA records of ref. 1 for forest land cover type. The correlation between the FRAP and these datasets is provided in *SI Appendix*, Table S1. The correlation significance is estimated using bootstrap resampling, where one of the two variables is shuffled 10,000 times and new correlations are computed.

Observed Climate Data. We use observational datasets of monthly precipitation and monthly mean of daily maximum near-surface air temperature (TS_{MAX}) obtained from the National Centers for Environmental Information database "nClimGrid", available at a spatial resolution of 5 km (49, 50). This data can be accessed at https://www.ncei.noaa.gov/data/nclimgrid-monthly/access/ (last access 22/11/2022).

We also consider the monthly mean VPD since ref. 1 showed that this is a key driver for fires in California. VPD was calculated from monthly temperature and dewpoint data from PRISM, available at a spatial resolution of 4 km (51). We used PRISM data because they provide all the variables needed to calculate the VPD. We used nClimgrid for precipitation and temperature since it has more strict record-length requirements than PRISM, making nClimgrid more appropriate for calculating multidecadal climate trends. In any case, the correlation of TS_{MAX} calculated with the two datasets is 0.99 (P value < 0.01).

For the purpose of our analysis, climate data were spatially averaged over the study domain.

Climate-Fire Model Derivation. First, we calculate the correlation between summer (May to September) log(BA) and different climate variables (maximum temperature, precipitation, and VPD) aggregated over different temporal windows (*SI Appendix*, Table S2). Very similar correlations have been obtained considering TS_{MAX} or VPD, with the highest value considering TS_{MAX} aggregated over the period from April to October (0.84).

Then, to derive the climate-fire model, we compare models employing monthly mean daily maximum temperature (TS_{MAX}) and precipitation (similarly to ref. 52). Prior to the analysis, the predictors are standardized by a) defining an anomaly by subtracting the long-term mean from the original series and by b) dividing the anomaly by its long-term SD. This standardization makes the coefficients of the regression model comparable with each other.

We consider all possible temporal aggregations of the predictors through a one-year out-of-sample calibration. Specifically, for temperature variables, we test all possible aggregations of multimonth series between January and October, while for precipitation, we also test antecedent periods starting from the previous October in order to capture potential mechanisms relating fuel moisture going into the fire

season. To identify the best model, we i) fit all the possible regression models considering all the potential predictors together or individually through a leave-one-year-out-cross-calibration; ii) calculate the significance of the individual (Pearson) correlations of these models through a one-tailed hypothesis test; iii) ensure that calculated correlations do not appear significant just by chance, by applying the false discovery rate method to adjust the *P* values of the correlation tests; iv) analyze the model with the highest correlation values among all the significant (adjusted *P* value < 0.01) correlations calculated in the previous steps. The most skillful model in predicting the May-to-September log(BA) is the one using April-to-October TS_{MAX} and July-to-September precipitation. However, only the coefficient of the TS_{MAX} predictor is statistically significant (*P* value < 0.01). *SI Appendix*, Fig. S2 *A* and *B* show a multiregression model that predicts BA from April to October TS_{MAX} and July to September precipitation. The model uses different subsets of the data or detrended fire and climate data. Results show that only the TS_{MAX} parameters are significant statistically, while the precipitation parameters are always not different from zero statistically. We also made another model that removed the effect of precipitation on TS_{MAX} by using a linear regression of precipitation and temperature series. We used this model on the observed temperature record to get another estimate of how precipitation and this adjusted TS_{MAX} are related to BA (*SI Appendix*, Fig. S2). In this case, the regression parameters are statistically significant (except considering the 25 coldest years for calibration; see *SI Appendix*, Fig. S2), and this model yields very similar results as the one that considers only TS_{MAX} as shown in Fig. 3 and *SI Appendix*, Fig. S5. We also test whether the model improves considering an interaction term between TS_{MAX} and precipitation, but the coefficient of this term is not statistically significant. Thus, in the following, we detail the development of the model that considers TS_{MAX}.

Specifically, we build a data-driven, empirical model that links the changes in summertime (May to September) BA over California to monthly mean maximum temperature (TS_{MAX}) aggregated over the period from April to October, as this is the temporal windows that maximize the correlation between TS_{MAX} and BA. We also include the month of October for TS_{MAX} aggregation since the FRAP fire records assign fires by the month they start and many of the fires in the region can continue to burn after September (generally until autumn rains limit flammability). The link between climate and BA is sought in the form of a log-linear stochastic model. In this formulation, BA is log transformed because BA has an exponential distribution. The simplest empirical model relating temperature in the year *i* to $\log(BA)_i$ assumes a linear dependence between the variables:

$$log\,(BA)_i = \beta_0 + \beta_1 \cdot TS_{MAX_i} + \sigma_r W_i, \qquad [\mathbf{1}]$$

where β_0 is the constant term of the regression model; the coefficient β_1 weights the temperature dependency. The last term represents the "residuals", i.e., the differences between the data and the deterministic version of the model. This is a noise term where σ_r^2 is the variance of the stochastic component, and Wi is white noise with zero mean and unit variance. To estimate the β coefficients of the model, we employ a standard least-squares method. Following standard procedures (see e.g., ref. 53), we tested that the stochastic term in the model is Gaussian (through the Kolmogorov–Smirnov test; 54), uncorrelated (through the Durbin–Watson statistic; 55) and does not present heteroscedasticity (through the Engle's ARCH test; 56).

The empirical model correctly reproduces the oscillations in the BA signal and the variance explained by the model amounts to about 71%. Bootstrap techniques are used to assess the significance of model parameter estimates. Specifically, we estimate the uncertainty of the parameters of the climate-fire model using bootstrap resampling, where the predictand and predictor pairs are drawn randomly with replacement 10,000 times and new regression models are fit to the data. The coefficient β_1 estimated fitting Eq. **1** is = 1.17 (0.96 to 1.37). Interpreting parameter estimates in a log-linear regression is not straightforward. For instance, consider increasing TS_{MAX} by one-degree Celsius, this means that

$$log\,(BA)_{new} = \beta_0 + \beta_1(TSmax + 1) = log(BA) + \beta_1.$$

Thus,

$$log(BA)_{new} - log(BA) = \beta_1,$$

or $e^{\beta_1} = BA_{new}/BA$ and d $100(e^{\beta_1} - 1)$ is the percent change in BA associated with a one-degree Celsius increase in TS_{MAX}, which consists of 222% (160 to 294%).

A stochastic component is usually introduced in empirical regression models to represent unresolved processes (53). Physically, the source of the stochastic term may account for stochastic factors like lightning outbreaks, wind events, and measurement errors (possibly in both BA and TS_{MAX} variables) and is also related to other processes that are not accounted for by the model. A stochastic component such as that included in Eq. **1** is a simplified way to describe these unresolved processes. This component is added following these steps: i) the variance of the residuals is estimated; ii) an ensemble of 10,000 Gaussian, temporally uncorrelated stochastic residual time series are generated, with variance equal to that estimated in the previous step; and iii) the stochastic residuals are added to the predicted model values, generating an ensemble of 10,000 predictions, which include the residual stochasticity.

It is also necessary to validate the quality and robustness of statistical models to perform out-of-sample prediction. To this aim, a leave-10-y-out cross-validation method was considered that divides the whole period into disjoint subperiods of 10 y (folds), and for each subperiod, the rest of the folds are used to train the model and to predict the corresponding 10-y subperiod (the last fold is of 11 y as it refers to the period 2011 to 2021). This procedure is repeated for each fold obtaining a prediction of the whole period considering training the model as an independent sample. Noticeably, the difficulty in obtaining a good out-of-sample prediction is higher than of a pure hindcast (reproduction) in which both the train and test periods are the same. Fig. 1 shows that this simple model can be used to produce out-of-sample 10-fold predictions of the BA response to climatic variability (correlation of 0.82, *P* value < 0.01). Clearly, the linearity of our model limits its applicability to conditions that are not too different from the current ones. A linear log(BA) response cannot be assumed under all situations, especially in the case of fuel limitation. However, in addition to the 10-fold cross-validation performed, we here provide more analysis to justify the applicability of this empirical model (*SI Appendix*, Fig. S2).

Climate Models. The list of climate models used is shown in *SI Appendix*, Tables S4 and S5. Historical and future projections of monthly mean near-surface daily maximum temperatures (tasmax) from the Coupled Model Intercomparison Project Phases 6 (CMIP6) were obtained from the User Data Gateway (https://meteo.unican.es/udg-tap/home) of the Santander MetGroup (https://meteo.unican.es). All the simulations were downloaded using the R climate4R package (https://github.com/SantanderMetGroup/climate4R, 57).

For the attribution analysis, we use two sets of simulations provided by the DAMIP under the umbrella of the CMIP6 initiative (36). Specifically, we use the "hist-nat" experiments that simulate the influence of natural forcing alone on the climate system (we call these runs CMIP6-NAT). These data cover the period until 2020. Since these are forced simulations, and not initialized from observations, for most variables, most years in the natural simulations are equivalent to each other (the only major exception to this is for the years following large volcanic eruptions). So as approximation, we concatenate the "hist-nat" experiment for 1971 to 2020 with a proxy for year 2021 using the mean of the data over the period 2001 to 2020. We also use the "historical" experiments (1971 to 2014) that simulate the influence of both human and natural forcings on the climate system (we call these runs CMIP6-ALL). Historical simulations with full forcings for 1971 to 2014 and from the SSP2–4.5 experiment for 2015 to 2021 have been concatenated together as stipulated by CMIP6. For the future scenario analysis, we use historical experiments and future scenarios (SSP2-4.5 and SSP5-8.5) for CMIP6 runs.

All the GCMs have been bilinearly interpolated to a common 1.0-degree horizontal resolution grid, and, as for the climate observations, we averaged the data of each model over the study domain. Then, the monthly GCM data have been aggregated over the period April to October, and finally, we applied equidistant quantile mapping (58) to each series considering as reference the observed data described above.

Model names and ensemble numbers are listed in *SI Appendix*, Tables S4 and S5. Importantly, simply averaging all ensemble members as ensemble mean would bias the result toward the models with more members; thus, we first apply the climate-fire model to each GCM realization, and then, we average across all the single model runs, before averaging across all the models.

In the attribution analysis, we used 137 simulations from 12 different GCMs, all of which "hist-nat," "historical," and "SSP2-4.5" experiments were available at the time of this analysis (*SI Appendix*, Table S4). For climate model data, VPD has been

calculated from mean minimum and maximum temperature and relative humidity considering all the models listed in *SI Appendix*, Table S4 except for the model BCC-CSM2-MR which does not provide all the necessary variables for calculating VPD.

In the analysis of future BA changes, we used 118 simulations from 24 different GCMs, for which "historical," "SSP2-4.5," and "SSP5-8.5" experiments were available at the time of this analysis (*SI Appendix*, Table S5).

For the attribution analysis, we computed the impact of anthropogenic climate change by nesting the model of Eq. **1** with CMIP6-NAT and CMIP6-ALL output data. When estimating the impact of anthropogenic climate change, the TS_{MAX} series (both observed and simulated) are rescaled to have the same mean value over the 23-y climatology centered around 1971 (1960 to 1982; similarly to ref. 37).

To reflect the joint statistical uncertainty from the climate-fire model and climate uncertainty arising from different GCMs, we nest Eq. **1** for each GCM, and we add an ensemble of 10,000 Gaussian, temporally uncorrelated stochastic residual time series, with variance equal to that estimated fitting Eq. **1** with observed data. With this approach, we generate an ensemble of 10,000 predictions × the number of GCMs used.

Similarly, to the attribution analysis, we calculate the future BA scenarios by nesting the model of Eq. **1** with CMIP6 data and generating an ensemble of 10,000 predictions × the number of GCMs used. This is a static model that does not incorporate vegetation feedbacks and assumes constant fuel extent. We constrain projections of the forest-fire area to 2050 recognizing the greater uncertainty in vegetation dynamics and human and climate trajectories after the midcentury. In addition, we test how fire-fuel feedbacks modify near-term forest-fire area using dynamic models that account for various fire-fuel feedbacks. Specifically, we estimate fire-fuel feedbacks considering the fraction of forested land that is unable to carry forest fire in a given year because it has been altered by recent fire or through semipermanent loss of forest due to postfire tree regeneration failure as in ref. 42. Assuming the broad range of uncertainty in the fire-fuel feedbacks, we present two forms of fire-fuel feedback: i) moderate constant and ii) moderate fading. In the case of the constant feedback, the limitations due to recent fire history are constant following fires, while the fading feedback more heavily weights the contribution from recent fires, and increasingly reduces the contributions from prior years. The term "moderate" indicates that we consider a moderate fuel-limitation strength to account for potential effects of past fires. For instance, in the moderate-constant fuel-limitation case, the forested area ineligible to burn postfire equals the total recent BA. The details of these models are described in ref. 43.

Data, Materials, and Software Availability. All data used in this study are publicly accessible. Data access links are included in the article. Software and data for reproducing the results of this study are available at https://github.com/marcoturco/2022_turco_pnas (60).

ACKNOWLEDGMENTS. We thank Benjamin D. Santer, Hideo Shiogama, and Nathan P. Gillett for their helpful comments. M.T. acknowledges funding by the Spanish Ministry of Science, Innovation and Universities through the Ramón y Cajal Grant Reference RYC2019-027115-I and through the project ONFIRE, grant PID2021-123193OB-I00, funded by MCIN/AEI/ 10.13039/501100011033. Y.Z. was supported by NOAA's Climate Program Office's Modeling, Analysis, Predictions, and Projections Program (grant NA20OAR4310426). S.J. acknowledges funding by the Spanish Ministry of Science, Innovation and Universities through the Ramón y Cajal Grant Reference RYC2020-029993-I. D.D.L. worked under the auspices of the US Department of Energy by Lawrence Livermore National Laboratory under Contract DE-AC52-07NA27344 and was funded by a UC-National Lab Collaborative Research and Training Awards on Mitigating and Managing Extreme Wildfire Risk in California (grant LFR-20-652467). A.A. acknowledges funding by the United States Department of Agriculture, the National Institute of Food and Agriculture Grant 2021-67022-35908. I.C. was supported by the La Caixa Foundation (Junior Leader Marie Skłodowska-Curie grant agreement no. 847648).

Author affiliations: [a]Department of Physics, Regional Atmospheric Modelling Group, Regional Campus of International Excellence Campus Mare Nostrum, University of Murcia, Murcia 30100, Spain; [b]Management of Complex Systems Department, University of California, Merced, CA 95343; [c]Applied Mathematics and Computer Science Department, University of Cantabria, Santander 39005, Spain; [d]Department of Atmospheric and Oceanic Sciences, University of California, Los Angeles, CA 90095; [e]National Atmospheric Release Advisory Center, Lawrence Livermore National Laboratory, Livermore, CA 94550-9698; [f]Department of Civil and Environmental Engineering, University of California, Irvine, CA 92697; [g]Department of Earth System Science, University of California, Irvine, CA 92697; and [h]ISGlobal–Barcelona Institute for Global Health, Barcelona 08003, Spain

1. A. P. Williams *et al.*, Observed impacts of anthropogenic climate change on wildfire in California. *Earth's Future* **7**, 892–910 (2019).
2. Cal FIRE, Top 20 largest California wildfires (2022). Available at: https://www.fire.ca.gov/media/4jandlhh/top20_acres.pdf.
3. P. E. Higuera, J. T. Abatzoglou, Record-setting climate enabled the extraordinary 2020 fire season in the western United States. *Glob. Change Biol.* **27**, 1–2 (2021).
4. H. Buechi, P. Weber, S. Heard, D. Cameron, A. J. Plantinga, Long-term trends in wildfire damages in California. *Int. J. Wildland Fire* **30**, 757–762 (2021).
5. M. Burke *et al.*, The changing risk and burden of wildfire in the United States. *Proc. Natl. Acad. Sci. U.S.A.* **118**, e2011048118 (2021).
6. J. T. Abatzoglou, A. P. Williams, Impact of anthropogenic climate change on wildfire across western US forests. *Proc. Natl. Acad. Sci. U.S.A.* **113**, 11770–11775 (2016).
7. M. L. Mann *et al.*, Incorporating anthropogenic influences into fire probability models: Effects of human activity and climate change on fire activity in California. *PLoS One* **11**, e0153589 (2016).
8. A. L. Westerling, Increasing western US forest wildfire activity: Sensitivity to changes in the timing of spring. *Philos. Trans. R. Soc. B Biol. Sci.* **371**, 20150178 (2016).
9. M. Goss *et al.*, Climate change is increasing the likelihood of extreme autumn wildfire conditions across California. *Environ. Res. Lett.* **15**, 094016 (2020).
10. S. Madadgar, M. Sadegh, F. Chiang, E. Ragno, A. AghaKouchak, Quantifying increased fire risk in California in response to different levels of warming and drying. *Stoch. Environ. Res. Risk Assess.* **34**, 2023–2031 (2020).
11. S. A. Parks, J. T. Abatzoglou, Warmer and drier fire seasons contribute to increases in area burned at high severity in Western US forests from 1985 to 2017. *Geophys. Res. Lett.* **47**, e2020GL089858 (2020).
12. A. L. Westerling, H. G. Hidalgo, D. R. Cayan, T. W. Swetnam, Warming and earlier spring increase western US forest wildfire activity. *Science* **313**, 940–943 (2006).
13. P. Morgan, E. K. Heyerdahl, C. E. Gibson, Multi-season climate synchronized forest fires throughout the 20th century, northern Rockies, USA. *Ecology* **89**, 717–728 (2008).
14. J. S. Littell, D. McKenzie, D. L. Peterson, A. L. Westerling, Climate and wildfire area burned in western U.S. ecoprovinces, 1916–2003. *Ecol. Appl.* **19**, 1003–1021 (2009).
15. R. Seager *et al.*, Climatology, variability, and trends in the U.S. vapor pressure deficit, an important fire-related meteorological quantity*. *J. Appl. Meteorol. Climatol.* **54**, 1121–1141 (2015).
16. A. L. Westerling *et al.*, Climate change and growth scenarios for California wildfire. *Clim. Change* **109**, 445–463 (2011).
17. J. K. Balch *et al.*, Warming weakens the night-time barrier to global fire. *Nature* **602**, 442–448 (2022).
18. A. A. Gutierrez *et al.*, Wildfire response to changing daily temperature extremes in California's Sierra Nevada. *Sci. Adv.* **7**, eabe6417 (2021).
19. Z. A. Holden *et al.*, Decreasing fire season precipitation increased recent western US forest wildfire activity. *Proc. Natl. Acad. Sci. U.S.A.* **115**, E8349–E8357 (2018).
20. R. A. Minnich, M. G. Barbour, J. H. Burk, R. F. Fernau, Sixty years of change in Californian conifer forests of the San Bernardino Mountains. *Conserv. Biol.* **9**, 902–914 (1995).
21. T. W. Swetnam, C. H. Baisan, "Historical fire regime patterns in the southwestern United States since AD 1700" in *Fire Effects in Southwestern Forest: Proceedings of the 2nd La Mesa Fire Symposium*, C. D. Allen, Ed. (Rocky Mountain Research Station: USDA Forest Service, 1996), pp. 11–32, http://digitalcommons.usu.edu/barkbeetles/85/.
22. J. R. Marlon *et al.*, Long-term perspective on wildfires in the western USA. *Proc. Natl. Acad. Sci. U.S.A.* **109**, E535–E543 (2012).
23. C. R. Dolanc, J. H. Thorne, H. D. Safford, Widespread shifts in the demographic structure of subalpine forests in the Sierra Nevada, California, 1934 to 2007. *Global Ecol. Biogeogr.* **22**, 264–276 (2013).
24. L. Harris, A. H. Taylor, Topography, fuels, and fire exclusion drive fire severity of the rim fire in an old growth mixed-conifer forest, Yosemite National Park, USA. *Ecosystems* **18**, 1192–1208 (2015).
25. S. A. Parks *et al.*, Wildland fire deficit and surplus in the western United States, 1984–2012. *Ecosphere* **6**, art275 (2015).
26. A. H. Taylor, V. Trouet, C. N. Skinner, S. Stephens, Socioecological transitions trigger fire regime shifts and modulate fire–climate interactions in the Sierra Nevada, USA, 1600–2015 CE. *Proc. Natl. Acad. Sci. U.S.A.* **113**, 13684–13689 (2016).
27. A. Klimaszewski-Patterson, P. J. Weisberg, S. A. Mensing, R. M. Scheller, Using paleolandscape modeling to investigate the impact of native American-set fires on Pre-Columbian forests in the Southern Sierra Nevada, California, USA. *Ann. Am. Assoc. Geogr.* **108**, 1635–1654 (2018).
28. J. T. Abatzoglou, C. M. Smith, D. L. Swain, T. Ptak, C. A. Kolden, Population exposure to pre-emptive de-energization aimed at averting wildfires in Northern California. *Environ. Res. Lett.* **15**, 094046 (2020).
29. N. Mietkiewicz *et al.*, In the line of fire: Consequences of human-ignited wildfires to homes in the U.S. (1992–2015). *Fire* **3**, 50 (2020).
30. J. G. Pausas, J. E. Keeley, Abrupt climate-independent fire regime changes. *Ecosystems* **17**, 1109–1120 (2014).
31. Y. Zhuang, R. Fu, B. D. Santer, R. E. Dickinson, A. Hall, Quantifying contributions of natural variability and anthropogenic forcings on increased fire weather risk over the western United States. *Proc. Natl. Acad. Sci. U.S.A.* **118**, e2111875118 (2021).
32. M. W. Jones *et al.*, Global and regional trends and drivers of fire under climate change. *Rev. Geophys.* **60**, e2020RG000726 (2022).
33. K. E. Taylor, R. J. Stouffer, G. A. Meehl, An overview of CMIP5 and the experiment design. *Bull. Am. Meteorol. Soc.* **93**, 485–498 (2012), 10.1175/BAMS-D-11-00094.1.
34. P. A. Stott *et al.*, Detection and attribution of climate change: A regional perspective. *Wiley Interdiscip. Rev. Clim. Change* **1**, 192–211 (2010).

35. N. L. Bindoff, P. A. Stott, X. Zhang, "Detection and attribution of climate change: From global to regional" in *Climate Change 2013: The Physical Science Basis. Contribution of Working Group I to the Fifth Assessment Report of the Intergovernmental Panel on Climate Change* (Cambridge University Press, Cambridge, UK and New York, NY, 2013).
36. N. P. Gillett *et al.*, The detection and attribution model intercomparison project (DAMIP v1. 0) contribution to CMIP6. *Geosci. Model Dev.* **9**, 3685–3697 (2016).
37. A. Ortiz-Bobea *et al.*, Anthropogenic climate change has slowed global agricultural productivity growth. *Nat. Clim. Change* **11**, 306–312 (2021).
38. J. T. Abatzoglou, A. P. Williams, L. Boschetti, M. Zubkova, C. A. Kolden, Global patterns of interannual climate-fire relationships. *Glob. Chang. Biol.* **24**, 5164–5175 (2018).
39. J. S. Littell, D. McKenzie, H. Y. Wan, S. A. Cushman, Climate change and future wildfire in the western United States: An ecological approach to nonstationarity. *Earth's Future* **6**, 1097–1111 (2018).
40. S. Matthews, Dead fuel moisture research: 1991–2012. *Int. J. Wildland Fire* **23**, 78–92 (2014).
41. K. E. Trenberth, D. J. Shea, Relationships between precipitation and surface temperature. *Geophys. Res. Lett.* **32**, L14703 (2005).
42. J. T. Abatzoglou *et al.*, Projected increases in western US forest fire despite growing fuel constraints. *Commun. Earth Environ.* **2**, 1–8 (2021).
43. P. F. Hessburg *et al.*, Wildfire and climate change adaptation of western North American forests: A case for intentional management. *Ecol. Appl.* **31**, e02432 (2021), 10.1002/eap.2432.
44. M. G. Rollins, LANDFIRE: A nationally consistent vegetation, wildland fire, and fuel assessment. *Int. J. Wildland Fire* **18**, 235–249 (2009).
45. A. D. Syphard, J. E. Keeley, Historical reconstructions of California wildfires vary by data source. *Int. J. Wildland Fire* **25**, 1221 (2016).
46. M. Krawchuk, M. Moritz, *Fire and Climate Change in California: Changes in the Distribution and Frequency of Fire in Climates of the Future and Recent Past (1911–2099)* (California Energy Commission, 2012).
47. J. Eidenshink *et al.*, A project for monitoring trends in burn severity. *Fire Ecol.* **3**, 3–21 (2007).
48. A. L. Westerling, A. Gershunov, T. J. Brown, D. R. Cayan, M. D. Dettinger, Climate and wildfire in the western United States. *Bull. Am. Meteorol. Soc.* **84**, 595–604 (2003).
49. R. S. Vose *et al.*, Improved historical temperature and precipitation time series for U.S. climate divisions. *J. Appl. Meteorol. Climatol.* **53**, 1232–1251 (2014).
50. R. S. Vose *et al.*, Gridded 5km GHCN-daily temperature and precipitation dataset (2015), 10.7289/V5SX6B56.
51. C. Daly *et al.*, Physiographically-sensitive mapping of temperature and precipitation across the conterminous United States. *Int. J. Climatol.* **28**, 2031–2064 (2008).
52. M. Turco *et al.*, Skilful forecasting of global fire activity using seasonal climate predictions. *Nat. Commun.* **9**, 1–9 (2018).
53. H. Tong, *Nonlinear Time Series: A Dynamical System Approach* (Oxford University Press, Oxford, 1990).
54. F. J. Massey Jr., The Kolmogorov-Smirnov test for goodness of fit. *J. Am. Stat. Assoc.* **46**, 68–78 (1951).
55. J. Durbin, G. S. Watson, Testing for serial correlation in least squares regression. *Biometrika* **37**, 409–428 (1950).
56. R. F. Engle, Autoregressive conditional heteroscedasticity with estimates of the variance of United Kingdom inflation. *Econometrica: J. Eco. Soc.* **50**, 987–1007 (1982).
57. M. Iturbide *et al.*, The R-based climate4R open framework for reproducible climate data access and post-processing. *Environ. Model. Software* **111**, 42–54 (2019).
58. H. Li, J. Sheffield, E. F. Wood, Bias correction of monthly precipitation and temperature fields from intergovernmental panel on climate change AR4 models using equidistant quantile matching. *J. Geophys. Res. Atmos.* **115**, D10101 (2010).
59. V. Eyring *et al.*, Overview of the coupled model intercomparison project phase 6 (CMIP6) experimental design and organization. *Geosci. Model Dev.* **9**, 1937–1958 (2016).
60. M. Turco *et al.*, Reproduction Materials for: Anthropogenic climate change impacts exacerbate summer forest fires in California. *Github* https://github.com/marcoturco/2022_turco_pnas. Deposited 18 April 2023.